Two-Dimensional Simulator for Propagation in Urban Environments

Danilo Erricolo, *Member, IEEE*, and Piergiorgio L. E. Uslenghi, *Fellow, IEEE*

Abstract— **A new 2D ray tracing simulator for EM propagation prediction in an urban environment is described. The new features are that no practical restrictions are imposed on the profile of the cross section connecting the transmitter to the receiver and that each surface is characterized by its own value for the surface impedance; also, second order diffraction coefficients for impedance wedges are used to allow for arbitrary values of the heights of both antennas. Comparisons with other methods and numerical results are presented.**

Keywords— **Urban areas, Geometrical theory of diffraction, Radio propagation, Electromagnetic propagation**

I. INTRODUCTION

THE topic of electromagnetic propagation inside urban environments is of great interest for wireless communications not only in well developed urban areas, but also in areas under development where the use of radio communication is cheaper than the installation of copper wire and fiber optics links. Earlier propagation models for radio communications were developed for long distances and obstacles were characterized as knife edges. Then multiple diffraction models were introduced to study the effects of many obstacles [1], but due to the difficulties of the numerical evaluation of the integrals that appear in the formulation of the problem, it was not possible to come up with a closed form expression [2]. Some authors extended the idea of using knife edge models to study urban environments [3-10] and the propagation phenomena were considered as diffraction past multiple screens. Furthermore, it became possible [11] to develop ray tracing models that account not only for diffractions but also for reflections.

Ray tracing models such as the one developed herein are superior to knife-edge models because the former can account for a detailed geometrical description of the environment; examples are found in [12-16]. Ray tracing models have been proposed for both three-dimensional and two-dimensional environments. Three-dimensional ray tracing models are usually of the kind referred to as Shooting and Bouncing Rays (SBR) methods, because each trajectory is traced, starting from the transmitter, and followed until an interaction occurs. The interaction is either a reflection from a surface or a diffraction at an edge. The analysis of a ray trajectory is concluded when either the ray passes close enough to the receiver or its distance from the receiver increases steadily. There is an important consideration related to SBR models. Any time a ray is incident on an edge, a cone of diffracted rays is created. Therefore, tracking all rays that undergo diffraction is not computationally possible, unless empirical assumptions are introduced to select some diffracted rays among those belonging to the diffraction cone. As a consequence, all SBR models are not capable of satisfying the law of edge diffraction without making additional assumptions that are not well grounded on physical principles. The great majority, if not all, of the contributions to three-dimensional ray tracing methods are limited by such assumptions, except for the work presented in [15] where rays are backtracked from the receiver to the transmitter. The latter is equivalent to specifying the positions of both transmitter and receiver and finding the trajectories connecting the two antennas, which is the approach taken in this paper. Two-dimensional ray tracing models are of two kinds: vertical plane models (i.e., rays propagate over the rooftops of buildings) and horizontal plane models (i.e., rays propagate around buildings). Two-dimensional models are still under investigations, as evidenced by [9], [17], [10]. With this paper, the authors provide new contributions to the area of vertical plane simulators for propagation in urban environments in terms of:
• a ray tracing algorithm that accounts for an arbitrary profile for the buildings;
• a propagation model that applies to arbitrary heights of both transmitter and receiver antennas;
• introducing impedance surfaces to electrically characterize the scatterers; and
• introducing second order diffraction coefficients for impedance wedges.

To the best of the authors' knowledge, no previous work has considered the use of second order diffraction coefficients for impedance wedges. The authors use them here to avoid the discontinuity of the fields at grazing aspects of incidence and observation. Specifically, this use deals with arbitrary values of antenna heights.
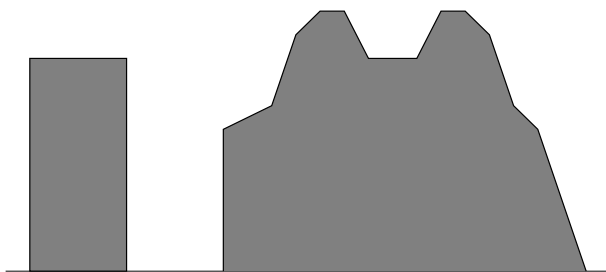

Fig. 1. Simple and complicated buildings.

In Section II, the assumptions for the development of the new algorithm are given, while the algorithm for the

determination of ray paths is explained in Section III. Section IV deals with the mathematical models for reflection, diffraction and free space propagation that are used to compute the attenuation of the field. Section V explains why knife edge models may be inappropriate for urban environments. Section VI motivates the advantages of the use of second order diffraction coefficients. Section VII presents a validation of this method by making a comparison with the method of the parabolic equation, with measurements, and the method of Zhang. In Section VIII a numerical example is discussed.

II. ASSUMPTIONS FOR THE 2D SIMULATOR

This new two-dimensional simulator analyzes the path loss experienced by electromagnetic waves that propagate through the obstacles of an urban environment using ray-tracing methods. Because it is a two-dimensional simulator, only the trajectories that are contained in a vertical plane passing through the transmitter and the receiver are considered. In addition, it is assumed that the vertical plane is normally incident on the walls of the buildings between the antennas. The profile of the obstacles that are cut by the vertical plane is represented by a polygonal line, so that both variations of the height of the terrain and complex building shapes, such as the one of Fig. 1, are taken into account. The new algorithm introduced into this simulator calculates all the rays that propagate along a vertical plane from the transmitter to the receiver, neglecting any backscattered ray (with one exception, to be discussed later).

Reflections can occur either on the terrain or along building surfaces. Diffractions are calculated using the Uniform Theory of Diffraction (UTD) and its extensions designed to account for scattering by impedance wedges. Each segment of the polygonal profile is associated with its own value of surface impedance so that varying electrical characteristics (boundary conditions) for both terrain and building surfaces are accounted for.
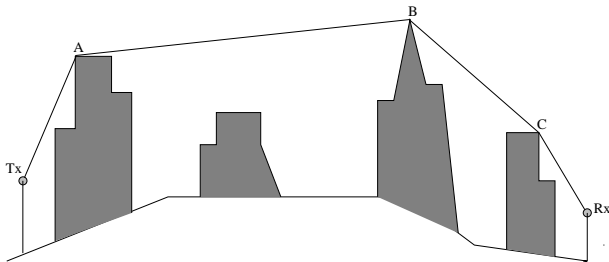

Fig. 2. City Profile.

III. 2D MODEL FOR RAY TRACING PROPAGATION

The two-dimensional simulator starts the analysis of the polygonal profile by looking for a line of sight (LOS) path between T_x and R_x. However, in practice the situations that are most likely to occur are similar to the one shown
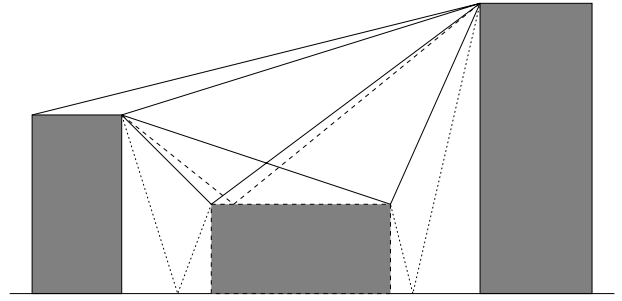

Fig. 3. Example of a subinterval.

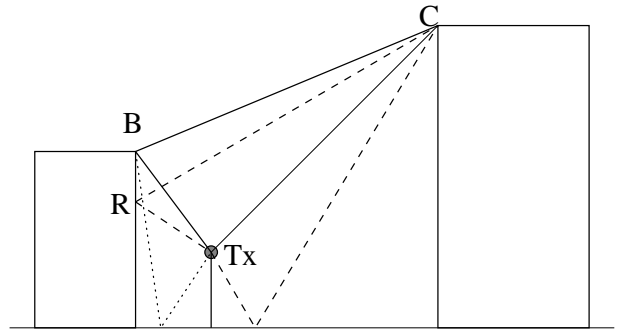in Fig. 2, where both variations in buildings and terrain height must be considered.

Fig. 4. Backpropagating rays.

The first step in the automatic generation of all the trajectories consists in finding the shortest path connecting T_x to R_x. This is accomplished by imagining a ribbon stretched on the top of the buildings so that, in the example of Fig. 2, the straight-line subpaths are: $T_x \rightarrow A$, $A \rightarrow B$, $B \rightarrow C$, $C \rightarrow R_x$. At this point it is worth noting that all the rays generated at T_x have to pass through point A in order to reach R_x. Points B and C behave similarly to point A. Whatever happens between A and B is independent of what happens between B and C, so the propagation process is summarized in the following way:

• All rays generated at T_x go to A.
• All ray paths reaching A go to B either directly or by diffraction/reflection on the obstacles between A and B.
• The same process applies between B and C.
• Finally R_x is reached from C either directly or by further diffraction and reflection.

The subsequent step is the study of each subinterval, so that all the ray paths going from the extreme left to the right are found; see Fig. 3 as an example. Inside each subinterval the algorithm checks whether any diffracting edge contributes to the creation of a path between the extremes of the subinterval. If so, it is taken into account. As an exception to what stated before, there is one situation when backscattered rays are considered and is depicted in Fig. 4.

The ray path $T_x \rightarrow R \rightarrow C$ might provide (especially if R lies on a strongly reflecting surface) a strong contribution
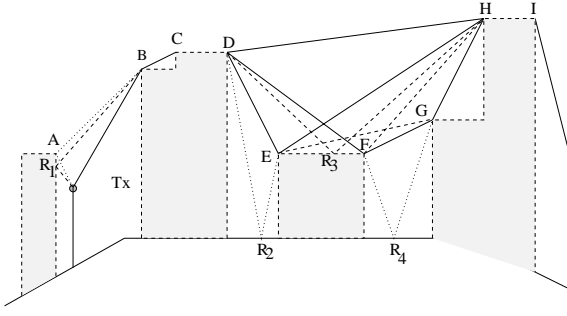
Fig. 5. A practical example.

to the field impinging on C because it only undergoes one reflection, therefore it is considered. For the same reason, $T_x \rightarrow B \rightarrow C$ is also taken into account. All the information about the subpaths is stored in a visibility graph, so that by reading it one can actually reconstruct all ray trajectories. A simplified example of a profile is shown in Fig. 5 and the corresponding visibility graph is given in Fig. 6.
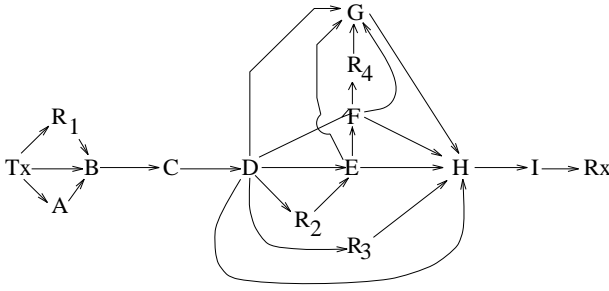

Fig. 6. Visibility Graph.

IV. MATHEMATICAL MODELS

The transmitter may be either a line source whose strength at a distance ρ from it is:

$$E(\rho) = \frac{e^{-jk\rho}}{\sqrt{\rho}} \ , \tag{1}$$

or a point source of strength:

$$E(\rho) = \frac{e^{-jk\rho}}{\rho} \ , \tag{2}$$

where k is the wavevector. Once a ray leaves the transmitter, there are two mechanisms that change the direction of propagation of a ray: reflection and diffraction. Reflections are accounted for by using the reflection coefficient for an impedance plane:

$$R = \frac{\sin\phi' - \sin\theta}{\sin\phi' + \sin\theta} \ , \tag{3}$$

where ϕ' is the angle between the surface and the incidence direction, and θ is a parameter related to the normalized

surface impedance η by:

$$\sin\theta = \left\{ \begin{array}{ll} 1/\eta & \text{for soft boundary} \\ \eta & \text{for hard boundary} \end{array} \right. \ . \tag{4}$$

In this two-dimensional simulator, diffraction is only caused by impedance wedges. Two kinds of diffraction mechanisms are considered: diffraction by simple wedges and diffraction by double wedges. Diffraction by simple wedges is computed using the coefficients reported in [18], [19]. Those coefficients apply to a plane wave perpendicularly incident on the edge of a wedge; however, they are used here for cylindrical and spherical wave incidence assuming that the incoming wave is locally plane when it reaches the edge. This assumption is approximately satisfied whenever the number of wavelengths between the source and the diffracting edge is large at the frequencies normally used for cellular communications inside cities. Therefore, the parameter L that appears in the formulation [19] is replaced with the UTD distance parameter that applies, for normal incidence, to cylindrical and spherical wavefronts, i.e.:

$$L = \frac{\rho\rho'}{\rho + \rho'} \ , \tag{5}$$

where the symbols are explained in Fig. 7. In the particular case of a wedge made of a perfect electrical conductor (pec), the coefficients given in [18], [19] reduce to the well known UTD coefficients reported in [20].
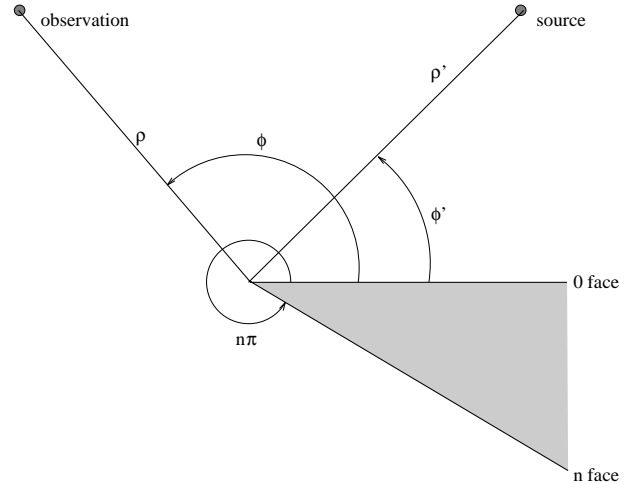

Fig. 7. Geometry for single impedance wedge diffraction.

Situations where both source and observation points are aligned with the common face of the double wedge, such as points T_x, Q, P and R_x in Fig. 15, deserve special attention. In fact, it is known [21] that the diffraction coefficient for a double wedge structure is not the product of two first order diffraction coefficients when one edge is in the transition zone of the other edge. Therefore, in order to retain the UTD approach, the use of a double wedge diffraction coefficient is required. In this way, all geometries with diffracting edges that are aligned with source and observation, such as those arising from arbitrary values of
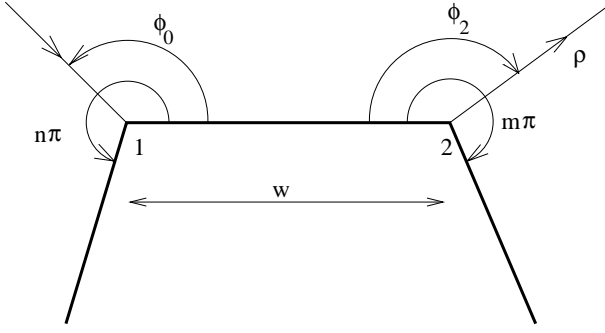
Fig. 8. Geometry for double impedance wedge diffraction.

antenna heights, are properly considered. Note that other authors have used an approach that combines UTD with physical optics [10], or UTD augmented with slope diffraction [22]; in this paper, only double wedge diffraction is considered to evaluate diffraction in the transition zones. In the literature, there are at least two different ways of expressing double-diffracted fields: one by Manara et al. [23] and the other by Herman and Volakis [24]. After a detailed study of the numerical behavior of both expressions, we concluded that the one proposed by Herman and Volakis was numerically preferable. Referring to Fig. 8, Herman and Volakis derived an expression for the field $u_{21}^d(\phi_0, \phi_2)$ diffracted first by edge 1, then by edge 2, where ϕ_0 and ϕ_2 are the incidence and observation aspects, respectively. Therefore, a double diffraction coefficient D^{II} was derived by writing expression (18) of [24] in the following form:

$$u_{21}^d(\phi_0, \phi_2) = D^{II}(\phi_2, \phi_0, n, m, w, k) \frac{\exp(-jkw)}{\sqrt{w}} \frac{\exp(-jk\rho)}{\sqrt{\rho}}$$

(6)

where n is the exterior wedge angle parameter at edge 1, m is the exterior wedge angle parameter at edge 2, w is the length of the common face, and k is the wavenumber. In the particular case of a double wedge made of a perfect electric conductor, the diffraction coefficients were taken from [25], [26].

The next step in the new simulator consists in the evaluation of the attenuation of the field due to the presence of obstacles. Let $E(T_x)$ and $E(R_x)$ be the electric field at the transmitter and receiver location, respectively. The overall electric field is the superposition of all the contributions due to the N paths at the receiver:

$$E(R_x) = \sum_{i=1}^{N} E_i(R_x) .$$

(7)

For each path i an attenuation factor is introduced in the following way:

$$A_i = \frac{E_i(R_x)}{E(T_x)} ,$$

(8)

so that the overall attenuation factor is:

$$A = \sum_{i=1}^{N} A_i$$

(9)

and (7) can be rewritten as:

$$E(R_x) = \sum_{i=1}^{N} A_i E(T_x) = E(T_x) A .$$

(10)

Each attenuation A_i is computed considering the contribution from free space propagation, first and second order diffraction coefficients at wedges, and reflections; its mathematical expression is:

$$A_i = \prod_{l=1}^{L_i} a_{il} \prod_{m=1}^{M_i} D_{im}^{(I)} \prod_{n=1}^{N_i} D_{in}^{(II)} \prod_{p=1}^{P_i} R_{ip} ,$$

(11)

where:
• a_{il} is the free space propagation due to the subpath l along path i.
• $D_{im}^{(I)}$ is the first order diffraction coefficient due to the edge m along path i.
• $D_{in}^{(II)}$ is the second order diffraction coefficient due to the double wedge n along path i.
• R_{ip} is the reflection coefficient due to the surface p encountered along path i.
• L_i, M_i, N_i, P_i are, respectively, the number of free space propagation subpaths, single impedance wedges, double impedance wedges and reflecting surfaces encountered along path i.
It is worth noting that each diffraction and reflection coefficient is a function of both incidence and diffraction angles as well as of the values of the surface impedance. All these factors are accounted for in the computer code. Additional details are found in [27].

V. COMPARISON WITH KNIFE EDGE MODELS

In this section, it is shown that an improvement is made by modeling obstacles with double wedges, instead of using knife edges, which are found in previous works [3-10]. The advantages of the double wedge approximation have already been introduced by these authors in [28]. The improvement brought with the double wedge approximation is demonstrated in a twofold way: 1) by comparing the overall attenuation for the double wedge and knife edge approximations; and 2) by computing the attenuation versus delay diagram for the two approximations. Referring to Fig. 9, where buildings are modeled using double wedges, the comparison is developed by computing the attenuation A (given by (9)) for the double wedge approximation and different possible knife edge approximations obtained by replacing each building of Fig. 9 with:
A) A knife edge that is located at the left wall of the building, see Fig. 10;
B) A knife edge that is located at the right wall of the building;
C) A knife edge that is located at the center of the building; and
D) Two knife edges, one in correspondence of the left wall and the other one in correspondence of the right wall.
All knife edges have the same height of the building that they approximate. It is worth noting that choices A) and
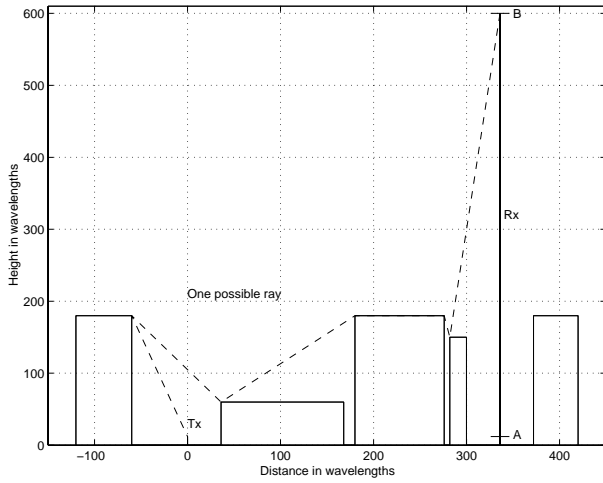
Fig. 9.   Profile for buildings approximated using double wedges.
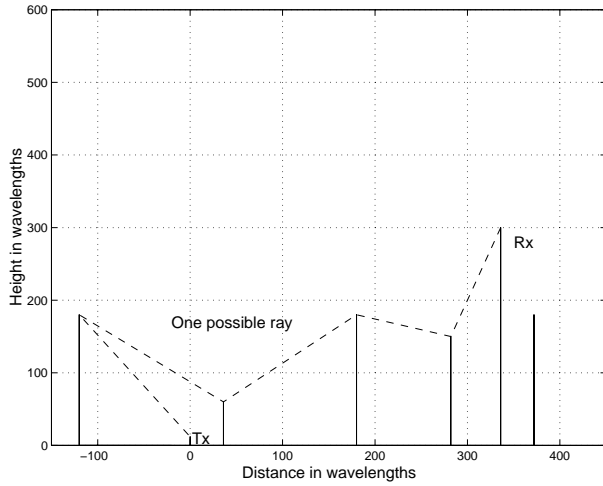

Fig. 10.   Profile for buildings approximated using knife edges located in correspondence of the left walls of the buildings of Fig. 9.

B) violate the reciprocity principle, since if T_x is switched with R_x the new situation is not reciprocal of the previous one. An automatic ray tracing for the profile shown in Fig. 9 was carried out and the receiver height was varied from A to B at small increments of $\lambda/10$ each. The results for perfect electrical conductor buildings and hard boundary are shown in Fig. 11.

One may notice that for large values of the antenna height the attenuation appears to settle at - 20dB. This is due to an LOS condition which is dominant; however one should keep in mind that there always is an attenuation due to free space propagation and -20dB is not a limiting value. Approximations D and E are close to each other when the height of R_x exceeds 300λ; however, in the range of heights between 300λ and 600λ all the knife edge approximations give an attenuation which is smaller compared to the double wedge approximation. This is due to the fact that, according to the kind of knife edge approximation (i.e. knife edge at the left, center or right of the building) the path between T_x and R_x might be considered

in LOS even though it actually is not, as shown in Fig. 12, where it is depicted what happens when the receiver height corresponds to 240λ.
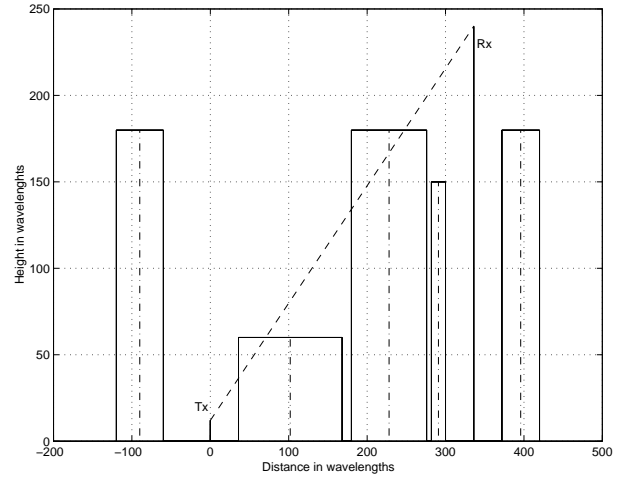

Fig. 12.   LOS condition.

It is worth pointing out that knife edge models usually neglect reflections and they are likely to yield incorrect results in terms of the intensity of the field received at antenna locations close to building walls.

The second comparison is carried out by analyzing the graph of the attenuation associated with each ray trajectory versus its delay time (i.e. the time it takes to a signal to propagate from T_x to R_x) for a fixed value of the receiver height. The attenuation versus delay diagrams are shown in Fig. 13 and in Fig. 14 for the knife edge model and the double wedge model, respectively.
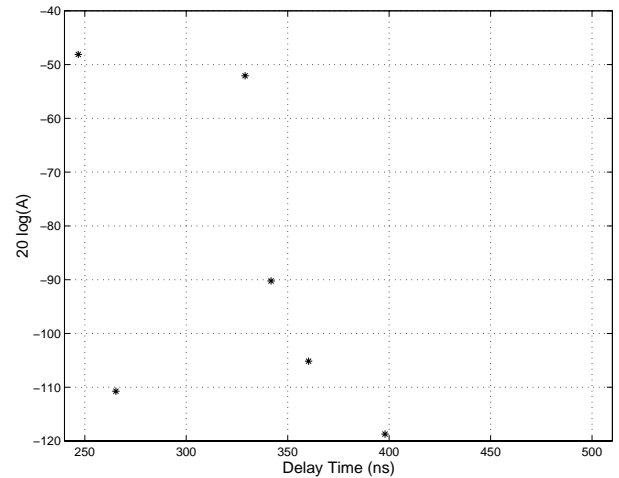

Fig. 13.   Attenuation versus delay for the knife edge model.

All knife edge approximations give similar diagrams and, therefore, only one is considered here. Keeping in mind that this is a theoretical comparison between two-dimensional models and that some of the attenuation values may be too large to be measured, it is instructive to observe that the number of multipath components that reach
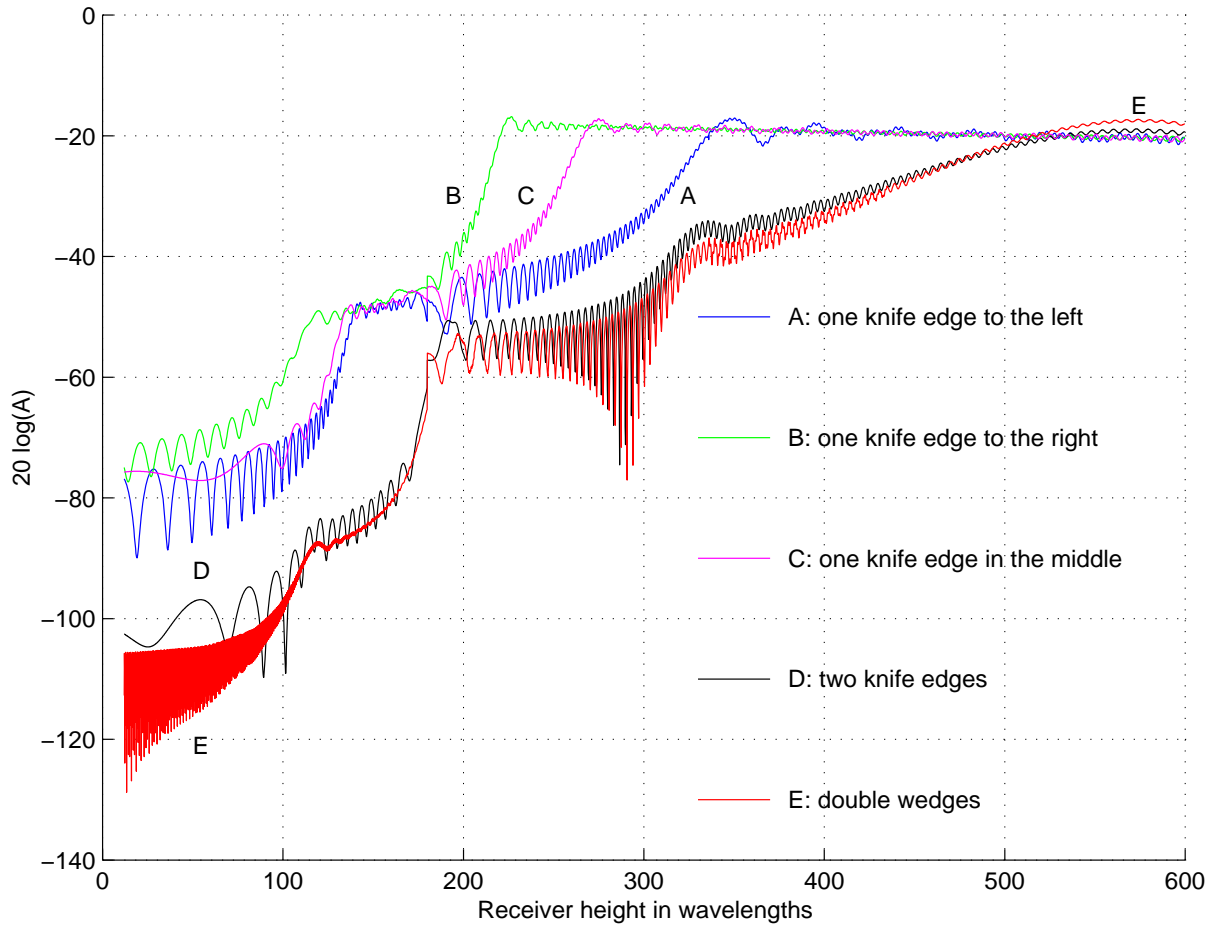
Fig. 11. Overall attenuation for the profile of Fig. 9 using different building models in the case of hard boundary. Results are shown for: A) One knife edge to the left; B) One knife edge to the right; C) One knife edge in the middle; D) Two knife edges; E) Double wedges.
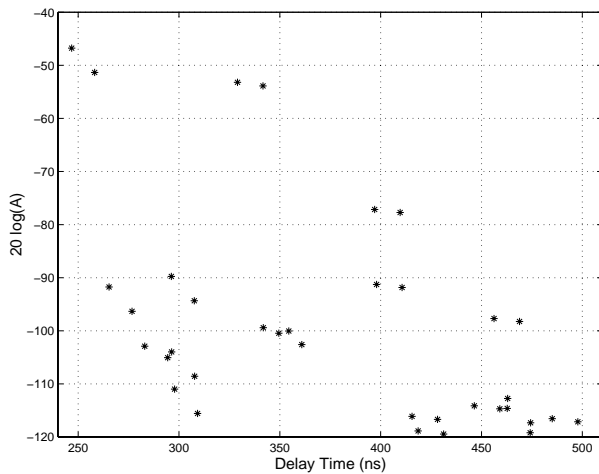

Fig. 14. Attenuation versus delay for the double wedge building model; profile of Fig. 9.

In particular, it is apparent that some multipath components that undergo a larger delay may have a smaller path loss than others that require a shorter time to propagate towards R_x. This last observation is important to determine the maximum delay time. For example, from Fig. 13 it appears that the maximum delay is about 400ns, whereas Fig. 14 shows that (due to other possible multipath components) the maximum delay is about 500ns. The maximum delay time is an important parameter for digital communications where it is strictly related to the bit transmission rate.

VI. IMPORTANCE OF THE SECOND ORDER DIFFRACTION MECHANISM

The use of a diffraction mechanism up to the second order allows the two-dimensional simulator to deal with arbitrary values of antenna heights. More specifically, the two-dimensional simulator can be applied to antenna heights above, near, and below the average building height because the second order diffraction coefficients graciously account for the appropriate behavior near the transition zones. In this section, an example of an antenna crossing the transition zone is carefully examined. Fig. 15 shows a double wedge structure where the wave emitted by the transmitter

R_x is larger in the case of the double wedge approximation. This larger number of multipath components comes from allowing into the computation of the trajectories both reflections from the rooftop of buildings and from the terrain.
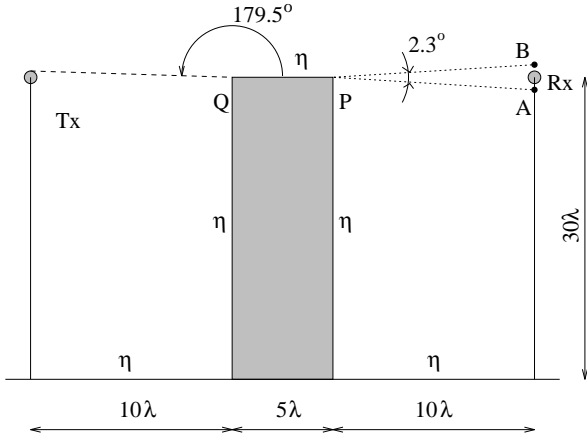
Fig. 15. Geometry for a double wedge obstacle at almost grazing incidence and observation aspects.
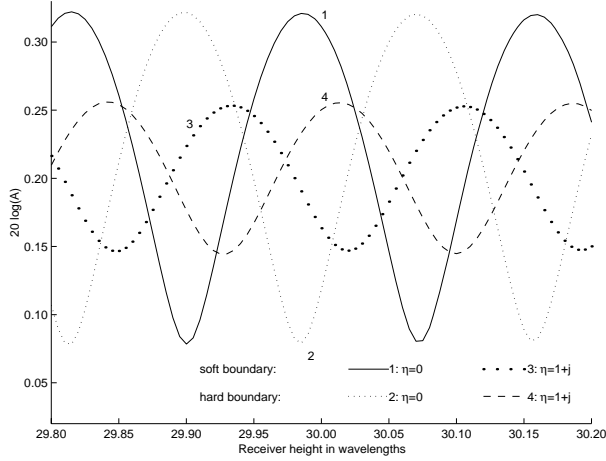

Fig. 16. Overall attenuation for the double wedge of Fig. 15 at grazing incidence and observation aspects. Results for $\eta = 0$ are shown in 1); for soft boundary and 2) for hard boundary; $\eta = 1 + j$ is considered in 3) for soft boundary whereas 4) represents the hard boundary case.

is impinging at almost grazing incidence on Q; the receiver is kept at a constant horizontal distance from P while its height is varied in such a way that R_x moves from A to B at small increments of $\lambda/200$ each. All surfaces have the same value of normalized impedance and the computed results for both $\eta = 0$ and $\eta = 1 + j$ are shown in Fig. 16 for both cases of soft and hard boundary. The results are clearly continuous and this is an important check to validate the algorithm for more complex situations. One should also note that when a second order diffraction coefficient is involved, not only the direct ray such as $T_x \rightarrow Q \rightarrow P \rightarrow R_x$ of Fig. 15 must be considered, but also $T_x \rightarrow P \rightarrow Q \rightarrow R_x$, as shown in Fig. 17. This is done to properly account for the correct field contributions and, therefore, the ray tracing algorithm must provide both kinds of trajectories.
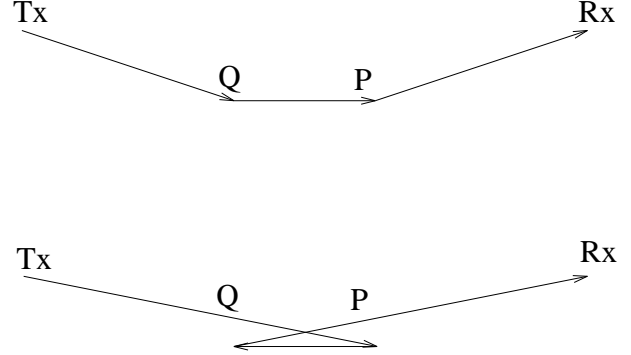

Fig. 17. Paths for second order diffraction.

VII. VALIDATION OF THE TWO-DIMENSIONAL SIMULATOR

In order to validate the two-dimensional simulator, its prediction is compared first with a different method based on the use of the parabolic equation, then with field measurements and finally with the method of Zhang. The geometry under exam is shown in Fig. 18, which shows an urban environment consisting of two pec rectangular buildings that have exactly the same height and are located on a pec terrain.
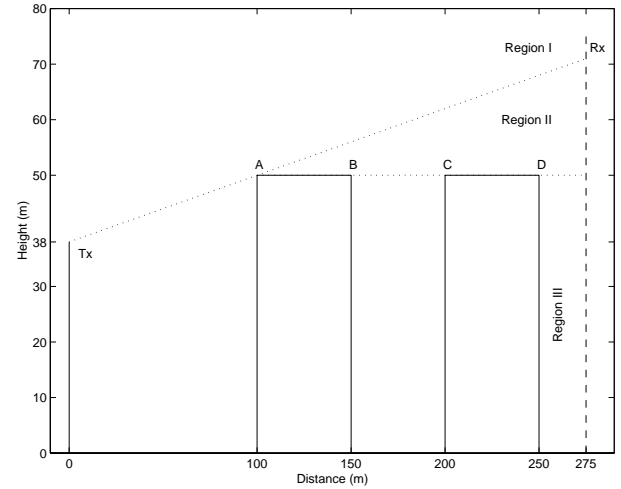

Fig. 18. Geometry for the comparison between the two-dimensional simulator and the parabolic equation method.

The building to the left is illuminated by a transmitter located below the common rooftop height. The receiver height is varied from values below, near and above the buildings height. Because the two buildings have exactly the same height, the field incident on C, after being diffracted by the double wedge AB is in its transition region. The situation depicted in Fig. 18 has been investigated in [29] using the parabolic equation method.

Fig. 19 shows the normalized field (i.e. the field normalized to the free space field) vs the receiver height, which is measured downwards from the roof of the buildings. The polarization is soft and the frequency is 970 MHz. The con-
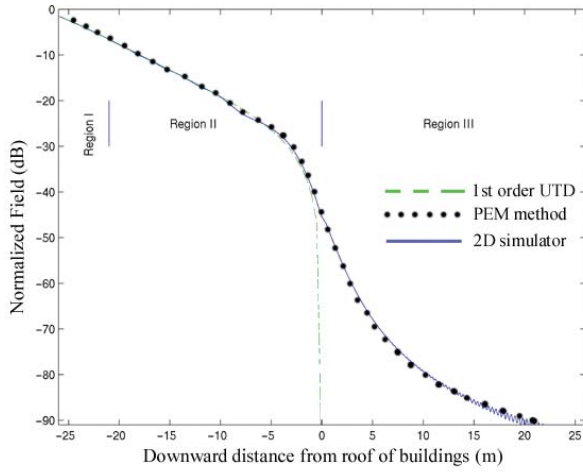
Fig. 19. Normalized field versus downward height for the geometry of Fig. 18. The continuous line represents the two-dimensional simulator result; the dotted line is the result obtained from the parabolic equation method as published in Fig. 8 of [29]. The dashed line represents the normalized field computed using a first order UTD ray-tracing approach.

tinuous line is the result of the two-dimensional simulator, whereas the dotted line (taken from one of the curves that appear in Fig. 8 of [29]) is the parabolic equation result. It is apparent that the agreement between the two curves is extremely good. When the receiver is located close to the terrain (downward height > 20m) there is an oscillation that is due to, referring to Fig. 18, the interference between the trajectory $D \to R_x$ with $D \to R \to R_x$. It is interesting to observe that in the parabolic equation method perfectly absorbing vertical walls are assumed. Nevertheless, the results are in perfect agreement, and this comparison proves the advantage of using a second order UTD when the diffracted fields are in their transition region. In addition, as a further motivation for the use of second order diffraction coefficients, the dashed line of Fig. 19 shows the prediction based solely on the first order UTD. Referring to Fig. 18, it is easy to understand that in Region I (LOS between T_x and R_x) and in Region II (LOS between T_x and R_x is obstructed only by the wedge A) the first order UTD in in agreement with the other theories. However, when R_x approaches Region III the diffraction coefficient for the diffraction at A vanishes and the first order UTD theory gives an erroneous null field in Region III.

As a second validation, a comparison with actual field measurements is now examined. The European committee COST 231 has published the results of many investigations about wireless communications. In particular, in [30] are reported the measurements for the environment of Hjørringvej, Denmark, which is reproduced in Fig. 20 and is sufficiently uniform in the direction transverse to the one of propagation to satisfy the two-dimensional assumption.

The measurements results are reproduced in Figures 21 and 22, together with the prediction of the two-dimensional simulator and an integral equation (IE) method discussed in [31]. In both cases, soft boundary and a frequency of
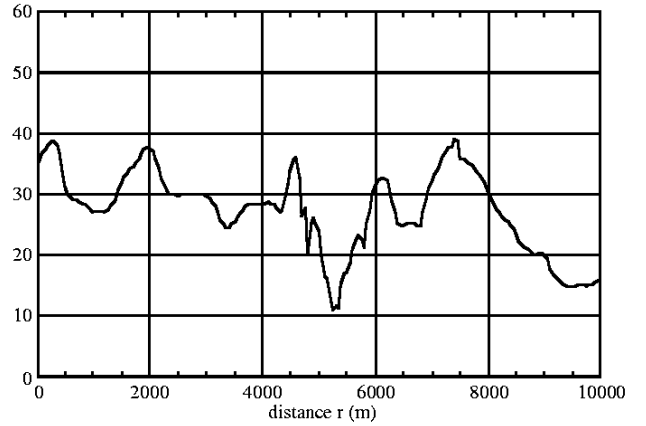

Fig. 20. Geometry for the terrain in the area of Hjørringvej, Denmark, as taken from Fig. 4.4.3 of [30]. This environment is fairly uniform in the direction transverse to the one of propagation to satisfy the two-dimensional assumption.
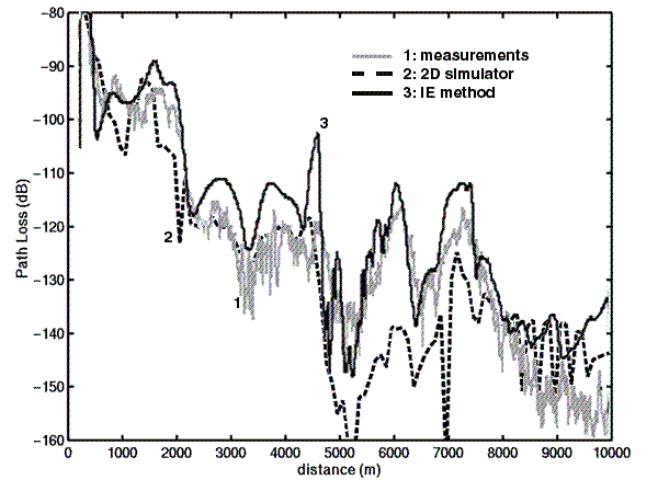

Fig. 21. Comparison of the path-loss obtained for the profile of Fig. 20 with: measurements (line 1), two-dimensional simulator (line 2), and Integral Equation method (line 3). A pec boundary condition is assumed for the terrain in the two-dimensional simulator.

970MHz have been considered. The difference between the two figures is in the boundary condition used by the two-dimensional simulator to analyze the terrain profile.

In Fig. 21 a perfect electric conductor (PEC) boundary condition is applied , whereas in Fig. 22 a perfectly absorbing (ABS) boundary condition was used. In both cases, there is good agreement between the two-dimensional simulator and the measurements. The mean error and the standard deviations for both the two-dimensional simulator and the integral equation method with respect to the measurements are shown in Table I. Referring to Fig. 21, where a perfect electric conductor boundary condition is used, the two-dimensional simulator tends to predict a stronger path loss than the measurements. In particular, for distance values between 2000m and 4000m, and between 7500m and 8500m the agreement with the measurements is very close. Referring to Fig. 22, where a perfect absorbing
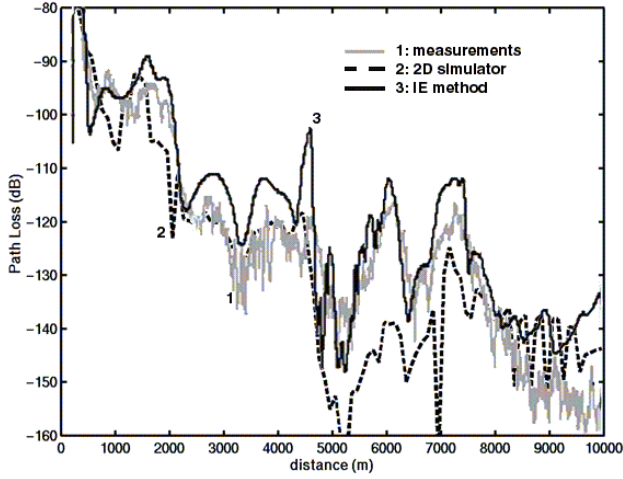
Fig. 22. Comparison of the path-loss obtained for the profile of Fig. 20 with: measurements (line 1), two-dimensional simulator (line 2), and Integral Equation method (line 3). A perfectly absorbing boundary condition is assumed for the terrain in the two-dimensional simulator.

TABLE I
MEAN ERROR AND STANDARD DEVIATION

	Mean Error	Standard Deviation
simulator (PEC)	2.3 (dB)	6.3 (dB)
simulator (ABS)	6.4 (dB)	14.9 (dB)
IE Method	6.4 (dB)	14.9 (dB)

boundary condition is used, the two-dimensional simulator predicts a stronger path loss for distances below 8000m, with a very close agreement between 2000m and 4000m. A comparison of the two-dimensional simulator results for the two different boundary conditions suggests that the perfect electric conductor boundary condition provides a closer overall agreement for the terrain profile of Fig. 20. Since for both boundary conditions the two-dimensional simulator provides a stronger path loss than the actual measurements, this suggests that there may be additional contributions that are not included in the vertical plane trajectories. Therefore, in the case of an actual three-dimensional environment, the prediction obtained with this simulator should provide a worst case path loss estimate. As a final comparison, the two-dimensional simulator is compared with Zhang's method, described in [9]. Zhang's method applies to the geometry shown in Fig. 23, where an urban environment consisting of parallel rows of buildings is simplified using parallel rows of perfectly conducting knife edges. The geometry of Fig. 23 is such that the transmitter is always above the rooftops height and the receiver is always in an obstructed area. The comparison is carried out by computing the total electric field at the receiver, while the receiver moves horizontally and d_r measures its distance from the knife edge to its left. The total field is
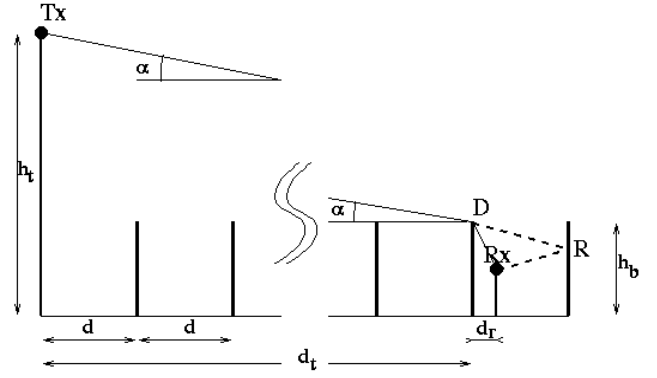
calculated assuming an isotropic source with transmitted power $P_t = 1$W and vertical polarization. Fig. 24 shows the

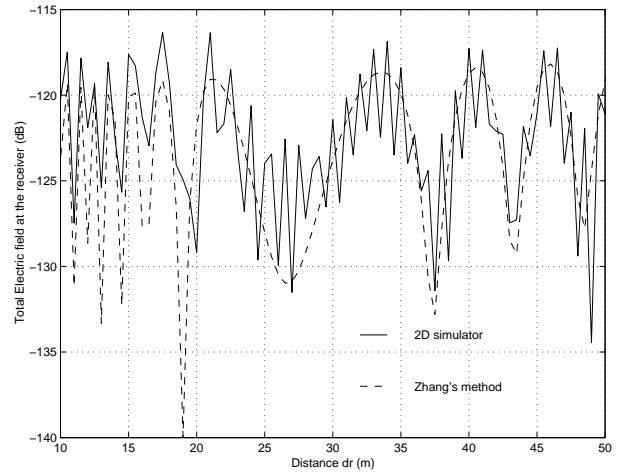Fig. 23. Geometry for the simplified urban environment.

Fig. 24. Comparison between the two-dimensional simulator (solid line) and Zhang's method (dashed line) for the simplified geometry of Fig. 23. The values used in the computation are: $f = 2.154$GHz, $h_t = 50$m, $d = 60$m, $d_t = 1020$m, $10 \leq d_r \leq 50$m, $h_r = 1.6$m, $h_b = 10$m, $\varepsilon_r = 5$; d_r varies at increments of 05.m, which corresponds to 3.6λ.

total electric field at the receiver versus the distance d_r for the case of transmitter height $h_t = 50$m, spacing between the knife edges $w = 60$m, building height $h_b = 10$m, number of knife edges between the transmitter and the receiver $n = 17$, frequency $f = 2.154$GHz. For this case, the slope of the path $T_x \rightarrow D$ corresponds to an angle $\alpha = 2.25°$. The solid line represents the two-dimensional simulator result and the dashed line is Zhang's prediction. For the simplified geometry under examination, there is good agreement between the two predictions. In fact, the mean difference between the curves is 0.75dB and the standard deviation is 4.1 dB. This agreement is more apparent when one compares the averages of the local values of Fig. 24. In fact, in Fig. 25, the difference between the average values of the two predictions never exceeds 3 dB. The local averages are computed from the data shown in Fig. 24 by replacing the local field magnitude $|E(x_i)|$ with the mean

of the values $|E(x_{i+j})|$ chosen within a window centered at x_i and with half-width 5m; for a frequency of 2.154GHz this is equivalent to an average over 36λ. The values of Fig. 24 were computed by varying the distance d_r from 10m to 50m at increments of 0.5m, which corresponds to 3.6λ. The boundary conditions for the two-dimensional simulator were chosen to resemble as much as possible Zhang's method. Therefore, a reflection coefficient $R = 0$ was introduced everywhere to avoid contributions from rays reflected from the ground level. All knife edges are perfect electric conductors and the knife edge to the right of R_x in Fig. 23 has a reflection coefficient computed assuming a dielectric material with $\varepsilon_r = 5$ (see [9]). The field computed by the two-dimensional simulator is multiplied by a factor $\lambda/4\pi$, where λ is the wavelength, so that the incident field given by Equation (2) is equivalent to the one used by Zhang. Because of the exact agreement between
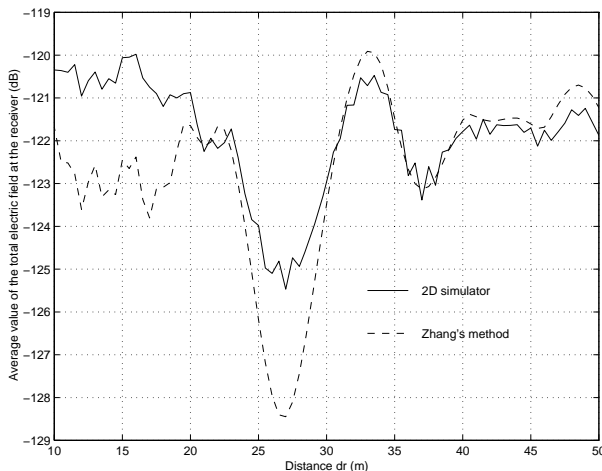

Fig. 25.   Comparison between the average values of the two-dimensional simulator (solid line) and Zhang's method (dashed line).

the two-dimensional simulator and the parabolic equation method, see Fig. 19, the close agreement with the measurements in Hjørringvej, and the agreement with Zhang's method we conclude that this two-dimensional simulator is reliable in terms of providing path loss predictions for the kind of two-dimensional environment described in Section II.

VIII. Numerical Results

As an example of an actual application of the new simulator, it has been applied to the profile cross section shown in Fig. 26. The overall attenuation (9) was computed for a receiver height varying from A to B at increments of $\lambda/10$. Six different conditions were examined and the results are shown in Fig. 27:
• Normalized surface impedance $\eta = 0$ for all the surfaces for both hard and soft polarization: curves 2 and 6.
• Normalized surface impedance $\eta = 1 + j$ for all the surfaces for both hard and soft polarization: curves 3 and 4.
• A composite situation with normalized surface impedance $\eta = 0$ on the roofs of the buildings only (i.e. between L

and M, N and O, P and Q, S and T) and $\eta = 1 + j$ on all other surfaces for both soft an hard polarization: curves 1 and 5.

In the case of perfect electrical conductors, the hard polarization provides the lowest attenuation, followed by the case in which only the roofs are perfect conductors. The other four cases are quite similar, even though the polarization conditions on the vertical walls are different. This suggests that the surface impedance that models the roof of a building is an important parameter, as already pointed out by these authors in [28].
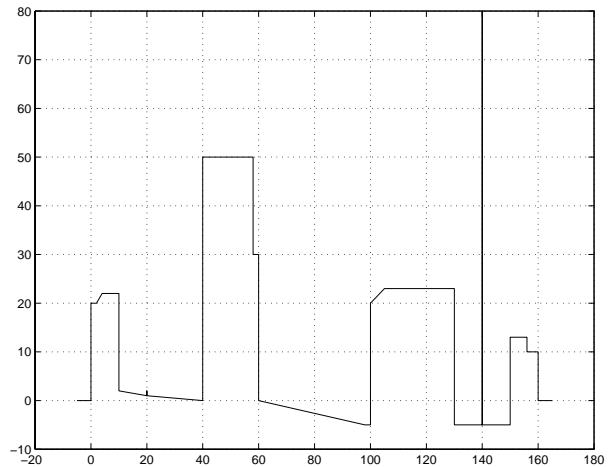

Fig. 26.   City profile; height of T_x is 12λ above ground.

IX. Conclusions

The advancement presented in this paper is the introduction of an algorithm that is capable of analyzing an arbitrary polygonal line profile, which is obtained by cutting an urban environment along a vertical plane. The new algorithm avoids restrictions usually present in other simulators such as uniform height of buildings, uniform spacing of buildings and flat terrain. A comparison with knife-edge models explains the reasons why the latter may be a source of errors for applications to urban environments. A comparison with the method of parabolic equation shows that by using second order diffraction coefficients the fields computed for antenna heights below, near, and above rooftops are correct. It is important to stress that the use of a second order diffraction coefficient is not merely a matter of using a more accurate mathematical formulation, but is necessary to avoid field discontinuities across optical boundaries. It should be noted that a different attempt to avoid such discontinuities was made using physical optics in [10] or slope diffraction in [22]. The overall ray tracing algorithm has to be properly designed to account correctly for doubly diffracted rays (see Fig. 17). Another feature of this simulator is the introduction of impedance surface that allows the examination of a wider class of electrical properties and not just the pec case. A comparison of this two-dimensional simulator with field measurements and Zhang's method completes the proof of the validity of
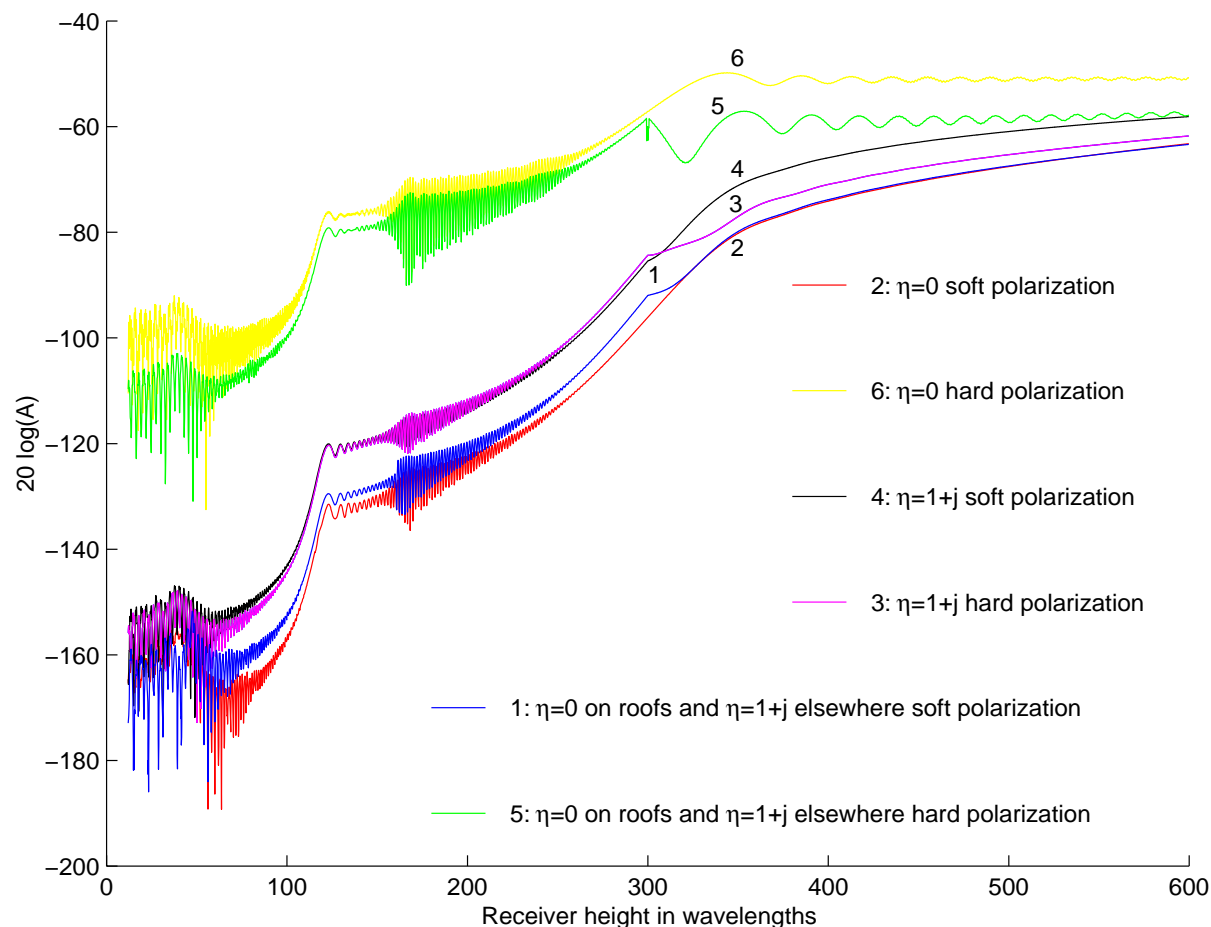
Fig. 27. Overall attenuation for the city profile of Fig. 26. Curves 2 and 6 represent, respectively, soft and hard polarization when $\eta = 0$; curves 4 and 3 represent soft and hard polarization when $\eta = 1 + j$; curves 1 and 5 represent soft and hard polarization when $\eta = 0$ on the roofs only and $\eta = 1 + j$ everywhere else.

this new method. Therefore, the limitations of this simulator are related to its two-dimensional nature. In summary, the salient feature of our work is the development of a fully automated code which does not require any in-depth knowledge of diffraction theory for its use. The only needed information is the input data: polygonal geometry and dimensions, frequency of operation, electrical impedance of each surface, and locations of transmitter and receiver.

ACKNOWLEDGMENTS

REFERENCES

[1] K. Furutsu, "On the theory of radio wave propagation over inhomogeneous earth," *J. Res. Nat. Bur. Stand., sec. D*, vol. 67, pp. 39–62, 1963.

[2] L. E. Vogler, "An attenuation function for multiple knife-edge diffraction," *Radio Sci.*, vol. 17, pp. 1541–1546, Nov-Dec 1982.

[3] J. Walfisch and H. L. Bertoni, "A theoretical model of UHF propagation in urban environments," *IEEE Trans. Antennas Propagat*, vol. 36, no. 12, pp. 1788–1796, December 1988.

[4] J-F. Wagen, "Sip simulation of UHF propagation in urban mi-

crocells," in *41st IEEE Veh. Technol. Conf.*, St. Louis, MO, USA, May. 1991, pp. 301–306.

[5] T. A. Russell, C. W. Bostian, and T. S. Rappaport, "A deterministic approach to predicting microwave diffraction by buildings for microcellular systems," *IEEE Trans. Antennas Propagat*, vol. 41, no. 12, pp. 1640–1649, December 1993.

[6] S. R. Saunders and F. R. Bonar, "Prediction of mobile radio wave propagation over buildings of irregular heights and spacings," *IEEE Trans. Antennas Propagat*, vol. 42, no. 2, pp. 137–144, February 1994.

[7] J-E. Berg and H. Holmquist, "An FFT multiple half screen diffraction model," in *1994 IEEE 44th Veh. Technol. Conf.*, Stockholm, June 8-10 1994, vol. 1, pp. 195–199.

[8] M. J. Neve and G.B. Rowe, "Mobile radio propagation prediction in irregular cellular topographies using ray methods," *IEE Proc. Microwave Antennas Propagat*, vol. 142, no. 6, pp. 447–451, December 1995.

[9] W. Zhang, "A wide-band propagation model based on UTD for cellular mobile radio communications," *IEEE Trans. Antennas Propagat*, vol. 45, no. 11, pp. 1669–1678, November 1997.

[10] W. Zhang, J. Lähteenmäki, and P. Vainikainen, "A Practical Aspect of Over-Rooftop Multiple Building Forward Diffraction from a Low Source", *IEEE Trans. Electromagnetic Compatibility*, vol. 41, no. 2, pp. 115–119, May 1999.

[11] F. Ikegami, T. Takeuchi, and S. Yoshida, "Theoretical prediction of mean field strength for urban mobile radio," *IEEE Trans. Antennas Propagat*, vol. 39, no. 3, pp. 299–302, March 1991.

[12] J. P. Rossi and A. J. Levy, "A ray model for decimetric radiowave propagation in urban area," *Radio Sci.*, vol. 27, no. 6, pp. 971–979, Nov-Dec 1992.

[13] T. Kurner, D. J. Chicon, and W. Wiesbeck, "Concepts and

overview," *IEEE J. Select. Areas in Commun.*, vol. 11, no. 7, pp. 1002–1012, September 1993.

[14] K. R. Schaubach and N. J. Davis IV, "Microcellular radio-channel propagation prediction," *IEEE Antennas Propagat Mag.*, vol. 36, no. 4, pp. 25–34, August 1994.

[15] M. F. Cátedra, J. Pérez, F. Saez de Adana, and O. Gutiérrez Blanco", "Efficient Ray-Tracing Techniques for Three-Dimensional Analyses of Propagation in Mobile Communications: Application to Picocell and Microcell scenarios", *IEEE Antennas Propagat Mag.*, vol. 40, no. 2, pp. 15–28, April 1998.

[16] G. Liang and H. L. Bertoni, "A New Approach to 3-D Ray Tracing for Propagation Prediction in Cities", *IEEE Trans. Antennas Propagat*, vol. 46, no. 6, pp. 853–863, June 1998.

[17] D. Erricolo and P. L. E. Uslenghi, "Two dimensional ray tracing simulator for radiowave propagation in urban areas with arbitrary building shape and terrain profile", *Proc. Intl. IEEE/URSI Symposium*, Atlanta, GA, USA", June 1998, p. 48.

[18] R. Tiberio, G. Pelosi, and G. Manara, "A uniform GTD formulation for the diffraction by a wedge with impedance faces," *IEEE Trans. Antennas Propagat*, vol. 33, no. 8, pp. 867–873, August 1985.

[19] T. B. A. Senior and J. L. Volakis, *Approximate boundary conditions in electromagnetics*, The Institution of Electrical Engineers, London, UK, 1995. Section 4.2.4.

[20] R. G. Kouyoumjian and P. H. Pathak, "A uniform geometrical theory of diffraction for an edge in a perfectly conducting surface," *Proc. IEEE*, vol. 62, no. 11, pp. 1448–1461, November 1974.

[21] S.-W. Lee, Y. Rahmat-Samii, and R. C. Menendez, "GTD, ray field and comments on two papers," *IEEE Trans. Antennas Propagat*, vol. 26, no. 2, pp. 352–354, March 1978.

[22] J. Bach Andersen, "UTD Multiple-Edge Transition Zone Diffraction" *IEEE Trans. Antennas Propagat*, vol. 45, no. 7, pp. 1093–1097, July 1997.

[23] G. Manara, R. Tiberio, G. Pelosi, P. H. Pathak, and R. G. Kouyoumjian, "Double Diffraction by wedges in non perfectly conducting surfaces," *Electron. Lett.*, vol. 23, no. 13, pp. 671–672, 18th June 1987.

[24] M. I. Herman and J. L. Volakis, "High frequency scattering by a double impedance wedge," *IEEE Trans. Antennas Propagat*, vol. 36, no. 5, pp. 664–678, May 1988.

[25] M. Albani, F. Capolino, S. Maci, and R. Tiberio, "Diffraction at a thick screen including corrugations on the top face," *IEEE Trans. Antennas Propagat*, vol. 45, no. 2, pp. 277–283, February 1997.

[26] F. Capolino, M. Albani, S. Maci, and R. Tiberio, "Double diffraction at a pair of coplanar skew edges," *IEEE Trans. Antennas Propagat*, vol. 45, no. 8, pp. 1219–1226, August 1997.

[27] D. Erricolo, "Wireless Communications in an Urban Environment" Ph.D. dissertation, Univ. Illinois at Chicago, Chicago, IL, USA, 1998.

[28] D. Erricolo and P. L. E. Uslenghi, "Knife edge versus double wedge modeling of buildings for ray tracing propagation methods in urban areas," in *Digest of National Radio Science Meeting*, Boulder, CO, USA, January, 1998, p. 234.

[29] R. Janaswamy and J. Bach Andersen, "Path loss Predictions in Urban Areas with irregular terrain topography" *Wireless Personal Communications*, vol. 12, pp. 255-268, 2000.

[30] T. Kurner "Propagation models for Macro-Cells," in *Cost 231, Evolution of land mobile radio (including personal) coomunications*, Final Report, Chap. 4, 1999.

[31] J. T. Hviid, J. Bach Andersen, J. Toftgård and J. Bøjer," "Terrain based propagation model for rural area- An integral equation approach," in *IEEE Transactions on Antennas and Propagation*, vol. 43, no. 1, pp. 45–46, January 1995.

Danilo Erricolo (S'97 - M'99) received the Laurea degree of Doctor in Electronics Engineering (summa cum laude) from the Politecnico di Milano, Italy, in 1993, and the Ph.D. degree in Electrical Engineering and Computer Science from the University of Illinois at Chicago, USA, in 1998. He is a research scientist with the College of Engineering of the University of Illinois at Chicago. His current interests are on the application of electromagnetic scattering to wireless communications. Dr. Erricolo was awarded twice both the Andrew Foundation Fellowship and the Beltrami Foundation Fellowship.

Piergiorgio L. E. Uslenghi (SM '70 - F '90) was born in Turin, Italy in 1937. He received the Doctorate in Electrical Engineering from the Polytechnic of Turin, and the M.S. and Ph.D. degrees in Physics from the University of Michigan, Ann Arbor in 1960, 1964 and 1967, respectively. He has been an Assistant Professor at the Polytechnic of Turin (1961), an Associate Research Engineer at Conductron Corporation, Ann Arbor, Michigan (1962-1963), and a Research Physicist at the Radiation Laboratory of the University of Michigan (1963-1970). In 1970, he joined the University of Illinois at Chicago, where he held a number of positions, including Founder and first Director of the Communications Laboratory (1976-1978), Founder and Director of the Electromagnetics Laboratory (1991-present), Professor of Electrical Engineering and Computer Science (1974-present), Associate Dean of the College of Engineering (1982-1987; 1994-present), and Acting Head of the Department of Electrical Engineering and Computer Science (1999-2000).

Dr. Uslenghi's research interests encompass antennas, microwaves, scattering theory and applications, modern optics, and applied mathematics. He has published five books and over 150 papers, is a past editor of Electromagnetics and of the IEEE Transactions on Antennas and Propagation, and has served for many years on the editorial boards of the Journal of Electromagnetic Waves and Applications, the European Journal of Telecommunications, and Alta Frequenza.

Dr. Uslenghi is a member of the Antennas and Propagation, Microwave Theory and Techniques, and Electromagnetic Compatibility Societies of IEEE. He served as Secretary-Treasurer, Vice-Chair and Chair of the Joint AP/MTT Chicago Chapter of IEEE twice, in 1975-1978 and in 1989-1992. He was the General Chair of the 1992 IEEE-APS International Symposium and URSI/NEM Meeting and the Organizer and Chair of the 1976 National Conference on Electromagnetic Scattering, both held in Chicago. He served as an elected member of the IEEE/APS Administrative Committee (1994-1996) and as Vice President (2000) and President (2001) of the IEEE Antennas and Propagation Society. He is a member of the Joint Committee on Future Symposia of IEEE/APS and USNC-URSI (1994-present), and was a member of the IEEE Heinrich Hertz Medal Committee (1992-1997). In 1990, he was elected Fellow of the IEEE for fundamental contributions to electromagnetic scattering theory and to engineering education.

Dr. Uslenghi was Chairperson of the Technical Activities Committee (1994-1996) and Vice-Chair (1997-1999) of USNC-URSI Commission B and is now Chair-Elect of Commission B (2000-2002). He is also a member of USNC-URSI Commission D. He has organized several special sessions at IEEE/APS International Symposia and URSI Meetings on such topics as nonlinear electromagnetism, scattering by wedges, advanced materials for electromagnetic applications, recent developments in scattering, and novel mathematical techniques in electromagnetics. He is the Chair of the Scientific Committee of the International Conference on Electromagnetics in Advanced Applications. He is a member of Phi Beta Kappa and Sigma Xi.